Although some biases could have existed because of the retrospective nature of our study, we feel that our data collection was accurate. First, we reviewed all ^{99m}Tc-MIBI scintigraphy studies performed in our institution during a well-defined period of time. Second, we reviewed the scintigraphic and pathologic data in a blind fashion with four independent expert observers (three nuclear medicine specialists and one pathologist).

CONCLUSION

Technetium-99m-MIBI uptake in the late phase of double-phase parathyroid scintigraphy is associated with a higher oxyphil cell content in parathyroid lesions (>25% or 50% of the total number of cells). No association was observed between other biological variables and the late uptake phase. On the other hand, uptake in the initial phase of the scan was associated positively with the volume of the lesion, serum calcium levels and diagnosis of primary hyperparathyroidism (parathyroid adenoma).

REFERENCES

1. Geatti O, Shapiro B, Orsolon PG, et al. Localization of parathyroid enlargement: experience with technetium-99m methoxyisobutylisonitrile and thallium-201 scintigraphy, ultrasonography and computed tomography. *Eur J Nucl Med* 1994;21:17–22.
2. Weber CJ, Vansant J, Alazraki N, et al. Value of technetium 99m sestamibi iodine 123 imaging in preoperative parathyroid surgery. *Surgery* 1993;114:1011–1018.
3. Rodriquez JM, Tezelman S, Siperstein AE, et al. Localization procedures in patients with persistent or recurrent hyperparathyroidism. *Arch Surgery* 1994;129:870–875.
4. Khan A, Samtani S, Varma VM, Frost A, Cohen J. Preoperative parathyroid localization: prospective evaluation of technetium 99m sestamibi. *Otolaryngol Head Neck Surg* 1994;111:467–472.
5. Hindié E, Melliere D, Simon D, Perlemuter L, Galle P. Primary hyperparathyroidism: is technetium 99m-sestamibi/iodine-123 subtraction scanning the best procedure to locate enlarged glands before surgery? *J Clin Endocrinol Metab* 1995;80: 302–307.
6. Thompson GB, Mullan BP, Grant CS, et al. Parathyroid imaging with technetium-99m-sestamibi: an initial institutional experience. *Surgery* 1994;116:966–973.
7. Casas AT, Burke GJ, Mansberger AR Jr, Wei JP. Impact of technetium-99m-sestamibi localization on operative time and success of operations for primary hyperparathyroidism. *Am Surg* 1994;60:12–17.
8. Taillefer R, Boucher Y, Potvin C, Lambert R. Detection and localization of parathyroid adenomas in patients with hyperparathyroidism using a single radionuclide imaging procedure with technetium-99m-sestamibi (double-phase study). *J Nucl Med* 1992;33: 1801–1807.
9. Taillefer R. ^{99m}Tc sestamibi parathyroid scintigraphy. In: *Nuclear medicine annual*. New York: Raven Press; 1995:51–79.
10. Bénard F, Lefebvre B, Beuvon F, Langlois MF, Bisson G. Rapid washout of technetium-99m-MIBI from a large parathyroid adenoma. *J Nucl Med* 1995;36:241–243.
11. Ghandur-Mnaymneh L, Kimura N. The parathyroid adenoma: a histopathologic definition with a study of 172 cases of primary hyperparathyroidism. *Am J Pathol* 1984;115:70–83.
12. O'Doherty MJ, Kettle AG, Wells P, Collins RE, Coakley AJ. Parathyroid imaging with technetium-99m-sestamibi: preoperative localization and tissue uptake studies. *J Nucl Med* 1992;33:313–318.
13. Wei JP, Burke GJ, Mansberger AR Jr. Prospective evaluation of the efficacity of technetium 99m sestamibi and iodine 123 radionuclide imaging of abnormal parathyroid glands. *Surgery* 1992;112:1111–1117.

Dual-Head Pinhole Bone Scintigraphy

Yong-Whee Bahk, Sung-Hoon Kim, Soo-Kyo Chung and June-Ho Kim
Samsung Cheil Hospital, Samsung Medical Center, Seoul; and Catholic University Medical College Hospitals, Seoul and Uijongbu, Korea

This article describes dual-head pinhole bone scintigraphy (DHPBS), which makes use of two opposing pinhole-collimated detectors to obtain one pair of magnified images of bone and joint at one time. The aims are to reduce scan time and solve the problem of the blind zone that is created in the background in single-head pinhole bone scintigraphy. **Methods:** DHPBS was used for normal hip and knee joints and one case each of lumbar spondylosis, vertebral compression fracture and pyoankle. The gamma camera used was a digital dual-head SPECT camera (Sopha Camera DST; Sopha Medical Vision International, Buc Cedex, France) connected to an XT data processor and a printer. Each of two opposing detectors was collimated with either a 3- or 5-mm pinhole collimator. The scan was performed 2–3 hr postinjection of 12–25 mCi ^{99m}Tc-oxidronate. Some 1500–2000 Kilocounts were accumulated at 15–40 min per pair. Anterior and posterior views were taken for the spine and hip and medial and lateral views for the knee and ankle. DHPBS images were correlated to radiographs. **Results:** DHPBS produced a pair of high-resolution bone and joint images at one time, reducing scan time by nearly half for each image. The paired DHPBS images clearly visualized both foreground and background objects, which effectively eliminated the blind zone. **Conclusion:** DHPBS can significantly improve efficiency and diagnostic acumen.

Key Words: dual pinhole scan; pinhole scan; bone imaging

J Nucl Med 1998; 39:1444–1448

The usefulness of single-head pinhole bone scintigraphy (SHPBS) is well established (*1–7*), and it is used increasingly for diagnosing a broad spectrum of skeletal diseases. However, it has two drawbacks. One drawback is the rapid falloff of radioactivity, which creates the nonvisualization or blind zone in the periphery of the field of view, and the other is low sensitivity with prolonged scan time. SPECT is a solution for the blind zone, although its resolution needs improvement (*8,9*). Most recently, pinhole bone SPECT has been introduced to enhance image resolution and diagnostic efficacy (*10*).

The radioactive falloff is proportional to the inverse square of the distance and the function of tissue absorption (*11*). In pinhole collimation, the falloff is more acute in the peripheries of the field of view. The peripheries of the field of view include not only the outer zone of the two-dimensional field on an X-Y coordinate but also the far zone on the Z-axis or the background that lies below the detector. In SHPBS, the background structures are almost not imaged at all due both to the falloff and the out-of-focus effect. Such a blind zone can be eliminated if a pinhole-collimated detector is placed close to the background side, either the anterior or posterior, or the medial or lateral aspect of anatomical structures such as the spine, hip, knee and ankle.

We describe dual-head pinhole bone scintigraphy (DHPBS) that produced an opposing pair of two high-resolution magnified images at one time that could visualize structures in both the foreground and background and eliminated the blind zone. This method can reduce the scan time by half for each image on average. Technically, DHPBS makes use of two 3- or 5-mm pinhole collimators to collimate two opposing detectors. Any dual-head gamma camera system may be used for DHPBS provided that the gantry has space to accommodate the patient after installing cone-and-pinhole-collimator (CPC) assemblies

Case no.	Age (yr)	Sex	Clinical diagnosis	Object	DHPBS projections
1	42	M	Normal control	Hip	Anterior/posterior
				Knee	Medial/lateral
2*	72	M	Spondylosis with sclerosis	Lumbar spine	Anterior/posterior
3	56	F	L1 compression fracture	Lumbar spine	Anterior/posterior
4	9	M	Pyogenic synovitis	Ankle	Medial/lateral

* Image-size equalizing zoom study case (Fig. 2).

in the two opposing detectors. Such CPC assemblies can be tailored to appropriate specifications.

MATERIALS AND METHODS

Patients

We performed DHPBS on one normal volunteer subject and on three patients with bone and joint diseases (Table 1). The normal subject was imaged for the baseline study of the hip and knee joints. The patient group included one case each of lower lumbar spondylosis with small spurs, compression fracture of the L1 upper end plate and acute pyogenic synovitis of the left ankle. In Case 2, imaging was performed to show improved visualization of the background anatomy as well as the electronic zoom effects that equalized image sizes and, in Case 3, to show the effects of pinhole-to-object distance (POD) adjustment for image-size equalization.

Gamma Camera System and Cone-and-Pinhole-Collimator Assembly

The gamma camera system used was a digital dual-head SPECT system (Sopha Camera DST; Sopha Medical Vision International, Buc Cedex, France) that was connected to an XT data processor (Version 3.30) and a thermal printer. Each of the two opposing detectors was collimated with a 3- or 5-mm pinhole collimator inserted in the tip of the adapter cone. We used 3-mm collimators in all but Case 2, in which the image-size equalizing zoom was tested using 5-mm pinhole collimators. Larger pinholes were needed to obtain two sets of DHPBS images within time limitations after intravenous injection of the radiopharmaceutical. The cone was 175 mm high, and the top and basal openings were 52 and 300 mm in diameter, respectively. The cone inclination was 55°. The system sensitivities of 3- and 5-mm low-energy pinhole collimators at 50 mm were 387 and 624 cpm/μCi, respectively and the system resolutions were 5.1 and 7.3 mm (FWHM), respectively. The maximum gantry-isocenter-to-detector distance was 330 mm, which was long enough to accommodate a patient in the supine or prone position on the scan table after installing the CPC assemblies (Fig. 1).

Dual-Head Pinhole Bone Scintigraphy

DHPBS imaging was started 2–3 hr after intravenous injection of from 12 (pediatric case) to 25 (geriatric case) mCi ^{99m}Tc-oxydronate. The radioactive counts accumulated and the scan time spent were dependent on the radioactivity available for the imaging, structure size and pinhole aperture, tissue thickness and density and POD (Table 2). Of these, POD and tissue thickness were the major factors, which varied according to the structures. For example, POD ranged from 0–4 cm (tabletop and mattress) or more in the knee and ankle and from 8–16 cm or more in the hip and spine, which are covered with thick adipose tissues and muscles in the gluteal region and abdominal wall, respectively. The lordotic curvature was another important POD determinant in the

lumbar spine. In obese patients, the abdominal wall was compressed by the collimated detector in order to reduce the POD. The POD difference between the two opposing detectors caused image-size inequality (Fig. 2A and B). However, the image sizes could be equalized by using either the zoom (Fig. 3) or adjusting the POD under CRT monitoring (Fig. 4). The appropriate zooming factor was about 1.3 for the lumbar spine. We used 5-mm pinhole collimators in Case 2 since more time was needed to obtain two pairs of DHPBS images to demonstrate the equalizing effect of the zoom.
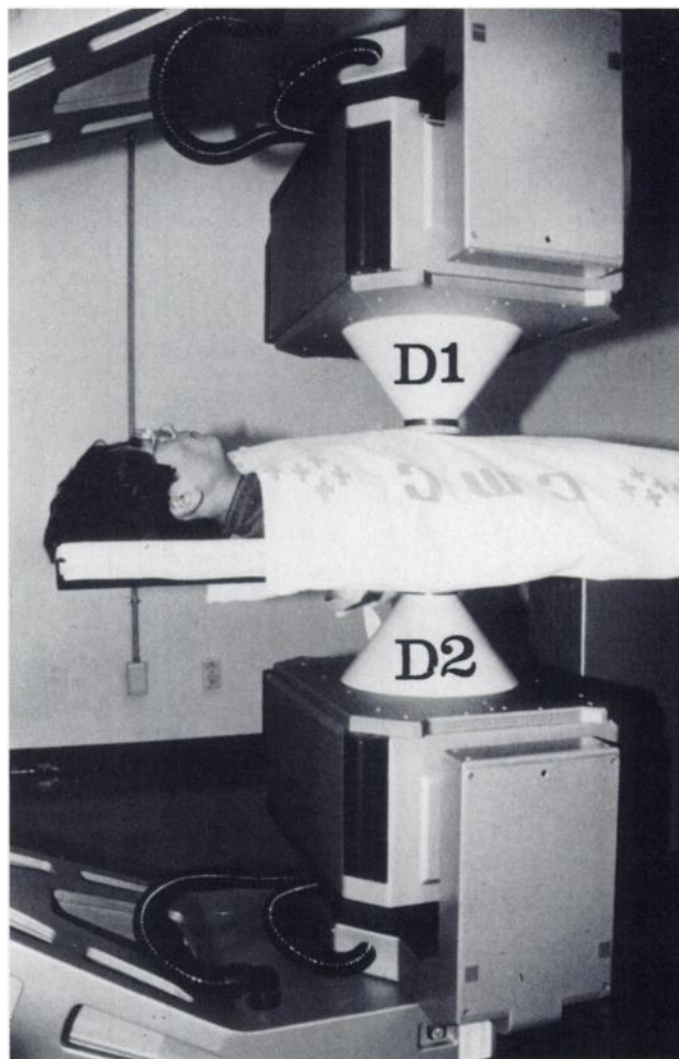
FIGURE 1. Dual-head pinhole bone scintigraphy in an operational position focusing on thoracolumbar spine. Each detector (D1, D2) is collimated with a cone-and-pinhole-collimator assembly.

TABLE 2
Scan Parameters of Dual-Head Pinhole Bone Scintigraphy for Various Anatomical Parts

Case no.	Anatomical part	Projection	Radioactivity (Kilocounts)*	Time/ pair (min)
1	Hip joint	Anterior	800	35
		Posterior	400	
	Knee joint	Medial	670	40
		Lateral	480	
2	Lumbar spine	Anterior	1000 (1100)†	40
		Posterior	1100 (1200)†	
3	Lumbar spine	Anterior	930	30
		Posterior	570	
4	Ankle	Medial	900	15
		Lateral	1100	

*The differences between paired projections are due to different pinhole-to-object distance and the size of the part covered.
†Increments required for zooming (×1.33).

RESULTS

As anticipated from earlier studies on SHPBS (1–7), the resolution and performance of DHPBS was satisfactory. It effectively reduced the scan time per image by half, and it eliminated the background blind zone of SHPBS by distinctly portraying the topography and pathological alterations in both the foreground and background of structures.

Case Reports

Case 1. Normal Hip and Knee Joints. The anterior DHPBS image of the hip joint clearly portrayed all important topographic landmarks, for example, the articular space (Fig. 2A) and the posterior image of the ischial spine (Fig. 2B). On the other hand, the lateral DHPBS image of the knee delineated the quadriceps tendon insertion at the midprepatellar facet (Fig. 2D), and the medial image delineated the infrapatellar tendon insertion at the patellar apex (Fig. 2E). The delineation of the tendon insertions was unique in that it does indicate the site of

increased bone metabolism. The DHPBS portrayal of anatomical landmarks was validated against radiographs (Fig. 2C, F).

Case 2. Lumbar Spondylosis with Small Spurs and Equalizing Zoom Technique. This case demonstrated both the improved image resolution and usefulness of the electronic zoom to equalize different image sizes of paired DHPBS. The image sizes may differ significantly according to the POD in asymmetric structures such as the spine and hip. The vertebrae shown on the anterior image were more greatly magnified and larger than those on the posterior image because the POD was closer anteriorly (Fig. 3, lower). Such image-size inequality was easily corrected by the zoom (Fig. 3, upper). As in the hip, the anatomical landmarks shown on the anterior and posterior images differed. For example, the anterior DHPBS image showed the anterior aspects of the end plates [Fig. 3, lower (A)] and the posterior image showed the spinous processes and facet joints [Fig. 3, lower (B)]. The image resolution in this case was relatively low compared to the others because the pinhole size was larger. Together, the anterior and posterior DHPBS images more completely portrayed the topography, thus solving the problem of the background blind zone. Several small spurs were visualized. Radiography was not available in this case, but the pinhole scan finding was typical (12).

Case 3. Compression Fracture of L1 Vertebra and Pinhole-to-Object Distance Equalization. This case showed, in addition to effective simultaneous coverage of both foreground and background structures, the effectiveness of the POD adjustment in equalizing image size. First, the anterior image showed an intense platelike tracer accumulation localized sharply in the upper end plate of L1 denoting a compression fracture (Fig. 4A). None of the posterior structures were shown on the anterior image. In contrast, the posterior image showed posterior anatomical landmarks as well as the posterior aspect of the fracture (Fig. 4B). The DHPBS findings were in agreement with the radiographic findings (Fig. 4C). Second, the sizes of the paired scan images could be equalized by moving the anterior detector from the ordinary POD farther away to the same POD
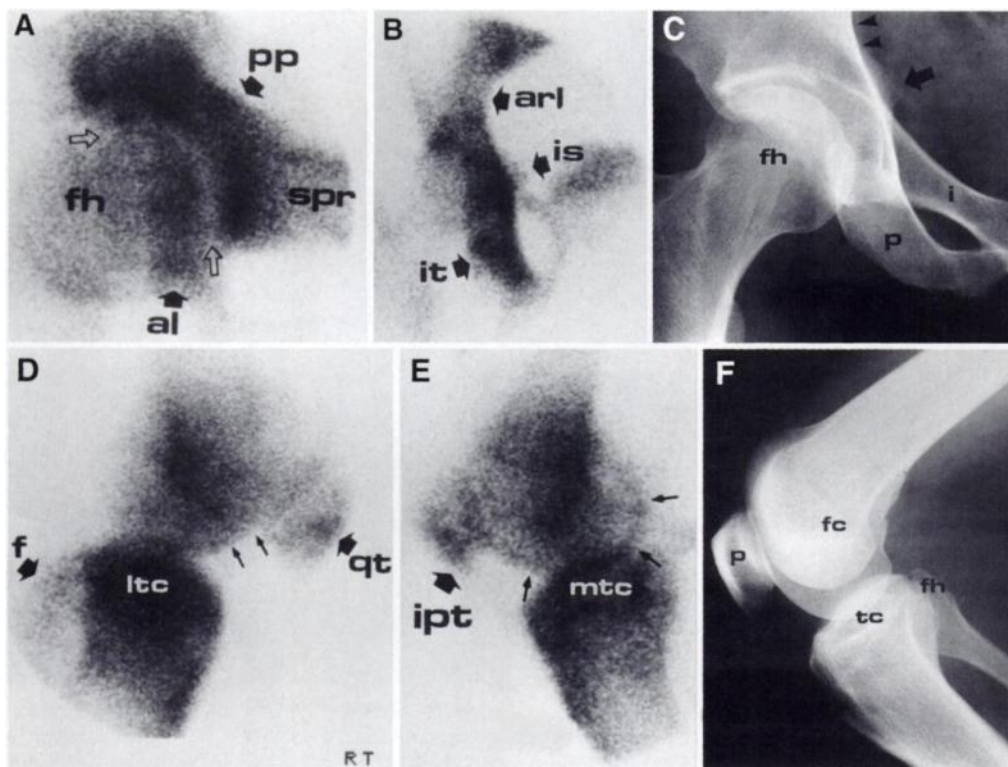

FIGURE 2. Dual-head pinhole bone scintigraphy images of normal hip and knee joints. (A) Anterior image of right hip joint portrays femoral head (fh), acetabular labrum (al), superior pubic ramus (spr) and pecten pubis (pp) as well as joint space (open arrows). (B) Posterior image portrays ischial tuberosity (it), ischial spine (is) and arcuate line (arl). (C) Anteroposterior radiograph identifies femoral head (fh), ischial tuberosity (i), pubic ramus (p), ischial spine, pecten pubis (arrow) and arcuate line (arrowheads). (D) Lateral image of right knee shows lateral femoral condyle (twin arrows), lateral tibial condyle (ltc) and fibular head (f). Note quadriceps tendon insertion is portrayed at central anterior surface (qt). (E) Medial image shows medial femoral condyle (small arrows), medial tibial condyle (mtc) and patella with infrapatellar tendon insertion at apex (ipt). (F) Lateral radiograph identifies femoral (fc) and tibial condyles (tc), fibular head (fh) and patella (p).
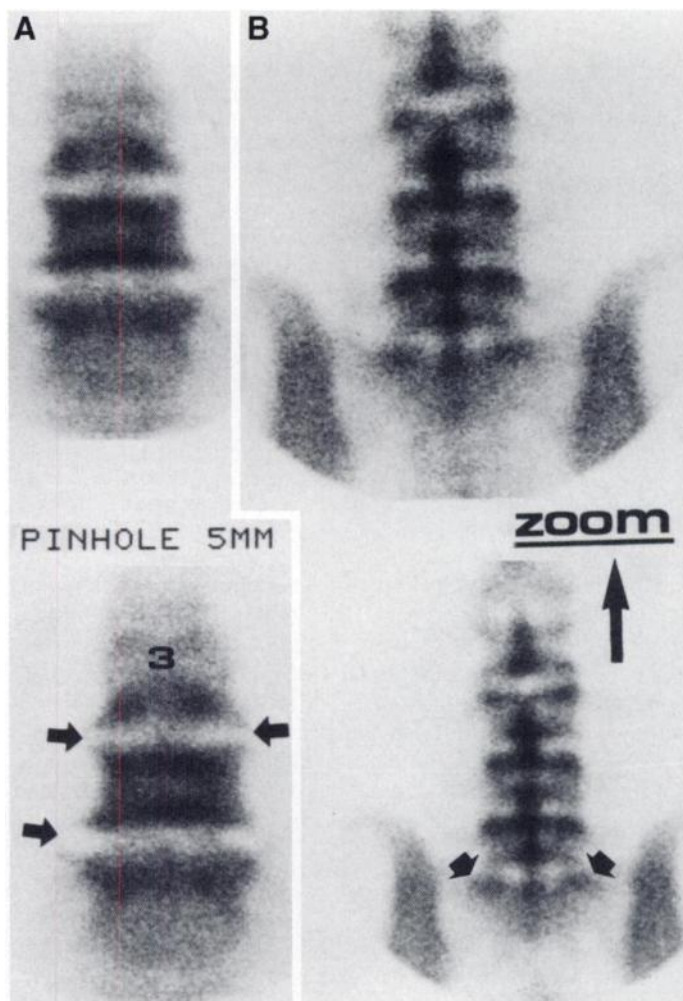
FIGURE 3. Zoom image-size equalization of lumbar spine. (A) (lower) Anterior and (B) (lower) posterior images are unequal in size with larger posterior image. (A) (upper) Anterior and (B) (upper) posterior image sizes are equalized by zooming posterior image by factor of 1.33. Anterior image portrays anterior disk spaces and vertebral end plates but not background anatomy and posterior image portrays posterior disk spaces and vertebral end plates along with spinous processes, facet joints (small arrows) and sacroiliac joints. Small spurs are visualized (large arrows).

FIGURE 4. L1 compression fracture and pinhole-to-object distance (POD) adjustment for equalizing image sizes. (A) Anterior dual-head pinhole bone scintigraphy image portrays intense platelike tracer accumulation localized in L1 upper end plate representing compression fracture (arrow). Posterior vertebral structures are not visualized. Incidentally, renal collecting systems are visualized. (B) Posterior image portrays posterior LI fracture (arrow) and spinous processes (arrowhead), facet joints (open arrows) and costovertebral joints (star). Two images cover foreground and background, eliminating blind zone. In this case, image sizes are equalized by equalizing PODs of two detectors under CRT monitoring. (C) Anteroposterior radiograph identifies spinous processes (arrowheads), costovertebral (star) and facet joints (open arrows) along with L1 upper end plate fracture (arrow).
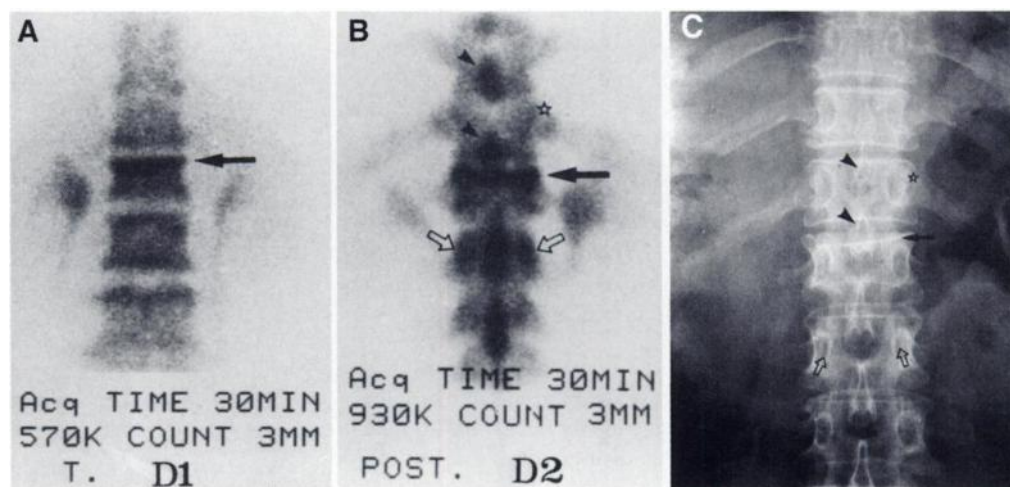

as the posterior detector under CRT monitoring (Figs. 4A and 4B).

Case 4. Acute Pyogenic Synovitis in the Ankle. The medial and lateral DHPBS images of the diffusely inflamed ankle revealed moderately increased tracer accumulation in the whole periarticular bones, giving rise to the classic wrapped bone sign of acute synovitis (*13*). The increased tracer accumulation was distributed typically in the synovial subchondral bones. The lateral and medial DHPBS images delineated the fibular malleolus and the anterolateral aspect of the talus (Fig. 5A) and the tibial malleolus and subtalar joint (Fig. 5B), respectively. The growth lines were distinctly imaged in the distal tibia and fibula. The wrapped bone sign was considered the scintigraphic version of the radiographic teardrop soft-tissue lobulation sign of acute pyogenic synovitis (Fig. 5C).

DISCUSSION

Pinhole magnification delineates both the anatomy and pathologic signs in detail, and it enhances diagnostic efficacy (*1–7*). It is now used increasingly to diagnose a wide variety of bone and joint diseases in both adults and children (*1,2*). However, it has two well-known drawbacks. The first is the acute peripheral falloff of radioactivity that creates image blurring and the blind zone and the second is the low sensitivity with its accompanying long scan time. The recent modification of the pinhole scan contributed to a shorter scan time (*1*), and SPECT is a solution for the blind zone, but the resolution still needs improvement (*8,9*). Recently, pinhole bone SPECT has been used to improve the resolution and contrast for both normal and pathologic bones (*10*).

Image blurring and the blind zone in the peripheries of the field of view are created by acute radioactivity falloff that is proportional to the inverse square of distance and tissue attenuation (*11*). These problems may also result from the out-of-focus effect of pinhole collimation. The falloff becomes exaggerated in pinhole magnification. On the other hand, the peripheries of the field of view are not limited to the outer zone of a two-dimensional field on the X-Y coordinate but to the far zone on the Z-axis. In clinical settings, the periphery on the Z-axis is the posterior aspect or the background of a structure opposing the foreground lying below the detector. In SHPBS, the foreground structures are the main images and the background structures are mostly not imaged, which results in the blind zone (Figs. 3 and 4). Such a blind zone can be eliminated
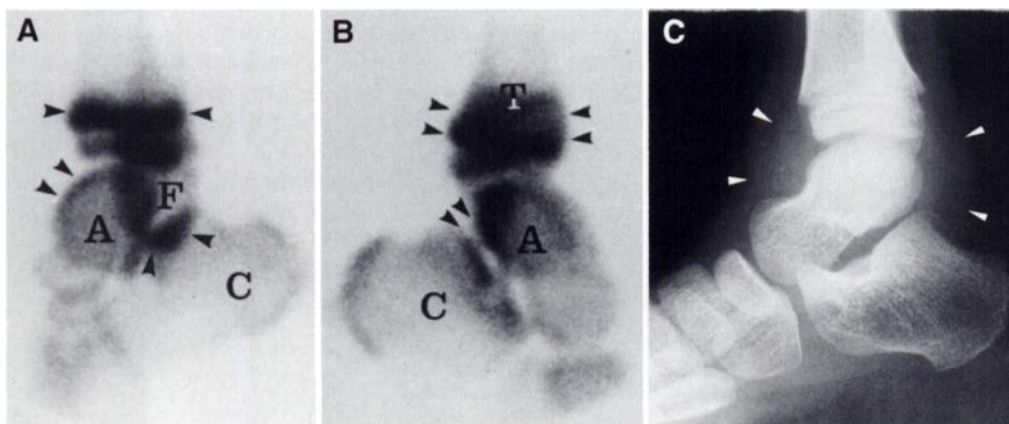
FIGURE 5. Three-dimensional dual-head pinhole bone scintigraphy (DH-PBS) presentation of diffuse inflammatory process of acute pyogenic synovitis in left ankle. (A) Lateral image portrays wrapped bone sign characterized by linear and curvilinear tracer accumulation in fibular malleolus (F) and lateral aspects of talus (A) and calcaneus (C) (lower arrowheads). (B) Medial image portrays similar alterations in tibial malleolus (T) and medial aspects of talus (A), calcaneus (C) and subtalar joint (lower arrowheads). Paired DH-PBS images can portray three-dimensional distribution of synovitis. Growth plates in distal tibia and fibula show intense tracer accumulation (upper arrowheads). (C) Lateral radiograph reveals diffuse capsular distension of synovitis, which is known as teardrop soft-tissue lobulation sign (arrowheads).

by placing a second detector close to the background side, either the anterior or posterior, or the medial or lateral aspect, of three-dimensional structures such as the spine, hip, knee or ankle.

We used DHPBS to image normal hip and knee joints and in one case each of lumbar spondylosis, compression fracture of the L1 vertebra and acute pyogenic synovitis of the ankle (Table 1). DHPBS was performed using dual detectors collimated with pinholes. This method demonstrated two obvious advantages. First, DHPBS produced a pair of high-resolution magnified images at one time, which reduced scan time by nearly half for each image on average. Second, the distinct portrayal of background structures effectively solved the blind zone problem created in SHPBS. In the hip joint, anterior and posterior images portrayed the anterior and posterior anatomic landmarks, respectively, as shown on Figures 2A and 2B. A similar effect was observed in the knee joint (Figs. 2D and 2E). It was unique that DHPBS was able to portray the subtle chemical profiles of increased tracer accumulation at the tendonous and ligamentous insertions of the patella. On the other hand, DHPBS showed spurs in lumbar spondylosis (Fig. 3) and an intense platelike tracer accumulation in a compression fracture (Fig. 4). Both the anterior and posterior structures of the spine were clearly visualized, which eliminated the blind zone. The paired DHPBS images of acute pyogenic synovitis of the ankle revealed the classic wrapped bone sign in a holistic way, which permitted the specific diagnosis (Fig. 5).

Technically, there are two basic requirements for successful DHPBS. One requirement is that there must be an adequate interdetector space after installing the CPC assemblies in the two opposing detectors. It must be large enough for the patient to be either supine or prone between the two pinhole-collimated detectors on the scan pallet. The other requirement is using the CPC assembly available as an option from the manufacturer. As to the pinhole size, we noted that both 3 and 5 mm are workable, although the former size is less sensitive and the latter has relatively low resolution. The optimal aperture size is 4 mm. The image sizes of paired DHPBS may differ according to different PODs. The inequality can be corrected by using either zoom or POD adjustments under CRT monitoring.

CONCLUSION

DHPBS can produce a pair of high-resolution bone and joint images at one time and reduce scan time by nearly half for each image. The paired DHPBS images of an anatomical structure clearly portray the topography of both the foreground and

background, effectively eliminating the blind zone. The pathological signs visualized on DHPBS images are three-dimensional and often quite specific. Technically, two requirements are to be met for successful DHPBS. These are an adequate interdetector distance and the use of a CPC assembly, which is available as an option from the manufacturer. As for pinhole size, we found 3 and 5 mm both workable, but the optimal size is 4 mm. The size inequality of the paired DHPBS images can be corrected by using either zoom or POD adjustments under CRT monitoring.

REFERENCES

1. Bahk YW. *Combined scintigraphic and radiographic diagnosis of bone and joint disease.* Heidelberg, New York: Springer-Verlag; 1994.
2. Treves ST, Connolly LP, Kirkpatrick JA, Packard AB, Roach P, Jaramillo D. Bone. In: Treves ST, ed. *Pediatric nuclear medicine,* 2nd ed. New York: Springer-Verlag; 1995:233–301.
3. Bahk YW, Kim OH, Chung SK. Pinhole collimator scintigraphy in the differential diagnosis of metastasis, fracture and infections of the spine. *J Nucl Med* 1987;28:447–451.
4. Yang WJ, Bahk YW, Chung SK, Choi KH, Jo KH, Jee MK. Pinhole skeletal scintigraphic manifestations of Tietze's disease. *Eur J Nucl Med* 1994;21:947–952.
5. Bahk YW, Park YH, Chung SK, Kim SH, Shinn KS. Pinhole scintigraphic signs of chondromalacia patellae in older subjects: a prospective assessment with differential diagnosis. *J Nucl Med* 1994;35:855–862.
6. Bahk YW, Park YH, Chung SK, Chi JG. Bone pathologic correlation of multimodality imaging in Paget's disease. *J Nucl Med* 1995;36:1421–1426.
7. Bahk YW. Pinhole scanning in tumors and tumorous conditions of bone: a new imaging approach to skeletal oncology. *J Orthop Sci* 1996;1:70–89.
8. Collier BD. Orthopaedic applications of single photon emission computed tomographic bone scanning. In: Fogelman I, ed. *Bone scanning in clinical practice.* London: Springer-Verlag; 1989:175–187.
9. Groch MW, Erwin WD, Bieszk JA. Single photon emission CT. In: Treves ST, ed. *Pediatric nuclear medicine,* 2nd ed. New York: Springer-Verlag; 1995:33–87.
10. Bahk YW, Chung SK, Park YH, Kim SH. Pinhole SPECT imaging in normal and pathological ankles. *J Nucl Med* 1998;39:130–139.
11. Sorenson JA, Phelps ME. The Anger camera: performance characteristics. In: Sorenson JA, Phelps ME, eds. *Physics in nuclear medicine.* 2nd ed. Philadelphia: W.B. Saunders Co.; 1987:338.
12. Bahk YW. Degenerative disease of the spine. In: Bahk YW. *Combined scintigraphic and radiographic diagnosis of bone and joint disease.* Heidelberg, New York: Springer-Verlag; 1994:85–91.
13. Bahk YW. Rheumatoid arthritis. In: Bahk YW. *Combined scintigraphic and radiographic diagnosis of bone and joint disease.* Heidelberg, New York: Springer-Verlag; 1994:100–101.